

Ferromagnetic resonance of a magnetic dimer with dipolar coupling

A. F. Franco, J. L. Déjardin, and H. Kachkachi

*Laboratoire PROMES CNRS UPR 8521, Université de Perpignan Via Domitia,
Rambla de la thermodynamique - Tecnosud, F-66100 Perpignan Cedex, France*

We develop a general formalism for analyzing the ferromagnetic resonance characteristics of a magnetic dimer consisting of two magnetic elements (in a horizontal or vertical configuration) coupled by dipolar interaction, taking account of their finite-size and aspect ratio. We study the effect on the resonance frequency and resonance field of the applied magnetic field (in amplitude and direction), the inter-element coupling, and the uniaxial anisotropy in various configurations. We obtain analytical expressions for the resonance frequency in various regimes of the interlayer coupling. We (numerically) investigate the behavior of the resonance field in the corresponding regimes. The critical value of the applied magnetic field at which the resonance frequency vanishes may be an increasing or a decreasing function of the dimer's coupling, depending on the anisotropy configuration. It is also a function of the nanomagnets aspect ratio in the case of in-plane anisotropy. This and several other results of this work, when compared with experiments using the standard ferromagnetic resonance with fixed frequency, or the network analyzer with varying frequency and applied magnetic field, provide a useful means for characterizing the effective anisotropy and coupling within systems of stacked or assembled nanomagnets.

I. INTRODUCTION

Today magnetic multilayers benefit from a renewed interest owing to the plethora of potential applications¹⁻⁶ they offer and the still challenging issues they raise for fundamental research^{7,8}. Among the latter, interlayer coupling is the focus of most of the investigations and debates as it constitutes one of the key physical parameters that determine the overall behavior and physical properties of the multilayer structures. For this reason, many theoretical and experimental investigations are carried out towards a better control of this parameter and a better understanding of its effect on the magnetization dynamics in magnetic multilayers. In particular, the nature of this coupling is of special interest and its characterization is still a target of intense investigation^{1,3,4,9-24}. Depending on the intrinsic properties of the constituting layers (underlying material, thickness, roughness, energy parameters, etc.) and the mutual interaction (chemical and physical), the interlayer coupling may change in nature and strength, leading to a variety of physical phenomena and applications.

On the other hand, assemblies of magnetic nanoparticles, deposited on a substrate or embedded in a matrix, provide another playground for various investigations, experimental and theoretical, with stimulating challenges both for fundamental research and practical applications²⁵⁻²⁹. Here, the coupling between pairs of nanoparticles is of paramount importance in the understanding of the dynamics of the system. During the last decades several approaches have been developed in order to fathom the role of inter-particle interactions in the onset of the macroscopic behavior of the assembly. Indeed, these interactions have a strong bearing on the distribution of the energy barriers, the relaxation rates, and the related dynamical observables such as the ac susceptibility³⁰⁻⁴² and hysteresis.

For the experimental investigation of either magnetic multilayers or assemblies of nanoparticles, there are nowadays many well-established techniques for precise measurements, such as the ferromagnetic resonance (FMR)^{20,43-46}, Brillouin Light Scattering (BLS)^{47,48}, and the ever developing optical and magneto-optical techniques⁴⁹⁻⁵³. The technique of FMR is one of the well established and easiest techniques^{20,43-46} that allows for a fairly precise probe of the magnetization dynamics, specially in magnetic hetero-structures. In the case of dipolar interacting magnetic elements, a comparison between theory and FMR spectrum provides us with a useful means to characterize the inter-elements coupling and help identify its origin and estimate its magnitude.

In this work, we accordingly investigate the FMR characteristics (resonance frequency and resonance field) of a magnetic dimer composed of two (identical) nanomagnets coupled by dipolar interactions (DI). The two magnetic elements are set up in either i) a vertical configuration thus modeling a multilayer with two magnetic layers separated by a nonmagnetic spacer, representing the generic situation that is relevant in spintronics⁵⁴, or ii) a horizontal configuration where the two magnetic elements form a pair of nanodisks or circular nanopillars⁵⁵, or still a pair of nanoparticles deposited on a substrate or embedded in a nonmagnetic matrix. We compute the resonance frequencies and the resonance fields upon varying the coupling strength and the direction and amplitude of the applied magnetic field, for various orientations of the anisotropy axes of the two magnetic elements. In this work, we investigate the effect of the dipolar coupling between the magnetic elements of finite

arXiv:1408.1594v1 [cond-mat.mtrl-sci] 7 Aug 2014

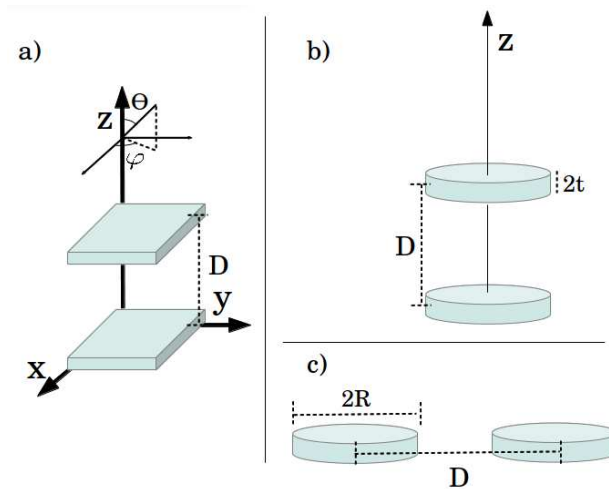


Figure 1: Setup of the magnetic dimer.

size, thus going beyond the standard dipole-dipole approximation for the magnetostatic energy.

The present work is organized as follows. In the next section we state the problem at hand and introduce the model for the magnetic dimer studied. Then, we establish the energy expression for the vertical and horizontal setup that takes account of the finite size and shape of the magnetic elements. In section III we derive the various expressions for the resonance frequency of the magnetic dimer (vertical or horizontal) for various configurations of the anisotropy axes (longitudinal, transverse and mixed). We plot the resonance frequency against the dipolar coupling or the applied field magnitude and the resonance field as a function of the applied field polar angle. We end this work with a conclusion of our main results and discuss further extensions thereof.

II. SYSTEM SETUP AND ENERGY

We consider a magnetic dimer composed of two identical ferromagnets, either two rectangular slabs or two thin cylinders. In the case of slabs we will consider the situation where they are arranged in a trilayer vertical stack with a nonmagnetic spacer. In this case, the centers of the three layers are along the z axis and the center-to-center distance between the two magnetic layers is henceforth denoted by D , see Fig. 1 a). This is a model for a multilayer system of two ferromagnetic thin films coupled via a nonmagnetic layer of a variable thickness. In Fig. 1 b) and c) we consider a pair of disk-shaped ferromagnets with centers either along the z axis or on the same plane $z = 0$, separated by a center-to-center distance D . The two disks (actually cylinders) have diameter $2R$ and thickness $2t$. The system of two disks mimics either multilayer samples as those used in spintronics⁵⁴ or a pair of nanodisks or circular nanopillars⁵⁵. The magnetic elements are ferromagnets with uniform magnetization, with in-plane or out-of-plane (effective) anisotropy, depending on their aspect ratio and underlying material.

In the case of a vertical setup (a or b) the two magnets are coupled via a nonmagnetic layer by a dipolar interaction (DI). For the horizontal set up 1 c) the two magnets are also coupled by the long-ranged dipolar interaction through, *e.g.* a nonmagnetic matrix or just air in the case of nanopillars. For the magnetostatic energy corresponding to the dipolar interaction, the induced magnetic state of the magnetic dimer depends on the orientation of the vector connecting the two magnets, the magnetic dimer bond, which is either along the z axis as in cases a) and b) or in the xy plane as in the case c).

In the sequel we will use spherical coordinates for all vectors involved. Hence, for the magnetic moments we write $\mathbf{m}_i = M_i \mathbf{s}_i$, with $M_i = M_0 V_i$, $\|\mathbf{s}_i\| = 1$ and $\mathbf{s}_i(\theta_i, \varphi_i)$, $i = 1, 2$. Since the two magnetic elements are supposed to be identical, $M_1 = M_2 = M$ will denote the saturation magnetization of each element. The applied field is $\mathbf{H} = (\mu_0 H) \mathbf{e}_h$, with $\|\mathbf{e}_h\| = 1$ and $\mathbf{e}_h(\theta_h, \varphi_h)$, and the anisotropy axes are denoted by $\mathbf{e}_i(\theta_i^a, \varphi_i^a)$, with $\|\mathbf{e}_i\| = 1$. The polar and azimuthal angles θ and φ are defined in Fig. 1.

We now write the energy of the magnetic dimer. Regarding the magnetic layers as being constituted by differential elements of volume dV carrying each the magnetic moment $d\mathbf{m}_i = M_0 dV \mathbf{s}_i$, $i = 1, 2$, the energy of the elementary magnetic moment $d\mathbf{m}_i$ may be written as

$$dE_i = \sum_{i=1,2} dE_i^{(\text{free})} + dE^{(\text{int})}$$

where $dE_i^{(\text{free})}$ is the energy of each individual (non-interacting) magnet that comprises the Zeeman and anisotropy contributions

$$dE^{(\text{free})} = - \sum_{i=1,2} \left[M_0 dV \mu_0 H (\mathbf{s}_i \cdot \mathbf{e}_h) + K dV (\mathbf{s}_i \cdot \mathbf{e}_i)^2 \right]$$

where K is the anisotropy constant.

As mentioned earlier, for each magnet the (effective) anisotropy axis is assumed to be unique (the same for all elements) and the magnetization is uniform. Therefore, integrating over the surface of each magnet leads to the total (intrinsic) energy (in S.I. unit) of the magnetic dimer

$$E^{(\text{free})} = - \sum_{i=1,2} \left[M \mu_0 H \mathbf{s}_i \cdot \mathbf{e}_h + K V (\mathbf{s}_i \cdot \mathbf{e}_i)^2 \right]. \quad (1)$$

It is convenient to measure this energy in terms of the anisotropy energy KV and accordingly introduce the (dimensionless) energy of the (free) magnetic dimer

$$\mathcal{E}^{(\text{free})} \equiv \frac{E^{(\text{free})}}{KV} = - \sum_{i=1,2} \left[2h \mathbf{s}_i \cdot \mathbf{e}_h + k (\mathbf{s}_i \cdot \mathbf{e}_i)^2 \right] \quad (2)$$

where we have introduced the dimensionless field parameter

$$h \equiv \frac{H}{H_a} \quad (3)$$

with

$$H_a = \frac{2KV}{M}$$

being the anisotropy field.

In Eq. (2) k is a simple “flag” merely introduced to keep track of the anisotropy contribution in later developments; it assumes the value 0 (1) in the absence (presence) of anisotropy, respectively.

The interaction contribution $dE^{(\text{Int})}$ for the elements $d\mathbf{m}_i$, considered here as point dipoles, is given by the standard dipole-dipole approximation

$$\begin{aligned} dE^{(\text{Int})} &= \left(\frac{\mu_0}{4\pi} \right) \frac{\rho^2 d\mathbf{m}_1 \cdot d\mathbf{m}_2 - 3 (d\mathbf{m}_1 \cdot \boldsymbol{\rho}) (d\mathbf{m}_2 \cdot \boldsymbol{\rho})}{\rho^5}, \\ &= \left(\frac{\mu_0}{4\pi} \right) d\mathbf{m}_1 \cdot \mathcal{D}_{12} d\mathbf{m}_2 \end{aligned} \quad (4)$$

where $\boldsymbol{\rho} = \mathbf{r}_1 - \mathbf{r}_2$ is the vector connecting the centers of the two magnets and \mathcal{D}_{12} the 2nd-rank tensor with

$$\begin{aligned} \mathcal{D}_{12}^{\alpha\beta} &\equiv \frac{1}{\rho^5} (\rho^2 \delta^{\alpha\beta} - 3 \rho^\alpha \rho^\beta) = \frac{1}{\rho^3} (\delta^{\alpha\beta} - 3 e_{12}^\alpha e_{12}^\beta) \\ \mathbf{e}_{12} &\equiv \boldsymbol{\rho} / \rho. \end{aligned}$$

For finite-size magnets the magnetostatic interaction energy involves the shape of the magnets with the help of appropriate shape functions^{56,57}. In the case of a vertical setup, either with oblong slabs or disks, it is well known that the dipolar interaction between two flat atomic planes of infinite lateral dimensions vanishes. In fact, this interaction would appear in principle only in the presence of roughness. However, because of boundary and finite-size effects the DI does exist between finite and flat planes (slabs and discs) and its intensity depends on the shape, the lateral size, and the distance between the two planes^{12,56,57}.

A. Rectangular slabs

In the case of two thin films, modeled here as two atomic planes of lateral dimension L and a distance D apart [Fig. 1a], the anisotropy field H_a in Eq. (3) may be written as $H_a = 2K_s/\sigma$ where σ is the magnetic moment per unit area. For cobalt, for instance, $\sigma = 1.7\mu_B/(0.5a^2)$, using the fact that the area a^2 contains two Co atoms, $a \sim 3.55 \text{ \AA}$ being the lattice step. The surface anisotropy constant K_s can be obtained from experiments on cobalt thin films^{8,58,59} for which it was evaluated to $K_s \simeq 0.5 \text{ erg/cm}^2 = 5 \times 10^{-4} \text{ J/m}^2$. So, $H_a \sim 4 \text{ T}$.

The energy of the DI is obtained by integrating Eq. (4) over the two planes leading to (the subscript ‘‘VS’’ stands for vertical slabs)

$$E_{\text{VS}}^{(\text{Int})} = \lambda \left[\cos(\varphi_1 - \varphi_2) s_1^\perp s_2^\perp - 2s_1^z s_2^z \right]. \quad (5)$$

with the coefficient

$$\lambda = \left(\frac{\mu_0}{4\pi} \right) \frac{M^2}{D^3} \times \mathcal{I}_s^v(\delta). \quad (6)$$

In Eq. (5), we have used the notation $\mathbf{s}_i(\theta_i, \varphi_i) = (s_i^\perp \cos \varphi_i, s_i^\perp \sin \varphi_i, s_i^z)$. $\mathcal{I}_s^v(\delta)$ is a (double) surface integral¹² whose analytic expression reads ($\delta \equiv \frac{D}{L}$)

$$\mathcal{I}_s^v(\delta) = 4\delta^3 \left[\delta - 2\sqrt{1+\delta^2} + \sqrt{2+\delta^2} + \frac{1}{2} \log\left(1 + \frac{1}{\delta^2}\right) + \log\left(\frac{1+\sqrt{1+\delta^2}}{1+\sqrt{2+\delta^2}}\right) \right].$$

For small values of δ the integral $\mathcal{I}_s^v(\delta)$ increases with δ as $4\delta^3 \left[\sqrt{2} - 2 + \log\left(\frac{2}{\delta(1+\sqrt{2})}\right) \right]$ while for large δ it does so as $1 - \delta^{-2} + 17\delta^{-4}/16$. We see that as the distance between the two magnets becomes very small, *i.e.* $\delta \rightarrow 0$, the integral $\mathcal{I}_s^v(\delta)$ and thereby the DI vanishes as it should. On the other hand, as the two magnets are very far apart, *i.e.* δ becomes very large, $\mathcal{I}_s^v(\delta) \rightarrow 1$ and thereby the dipolar interaction reaches the limit of the dipole-dipole approximation of point dipoles. This behavior is clearly seen in Fig. 2.

Eq. (5) then gives the energy of interaction between two identical planes uniformly magnetized in arbitrary directions. In the particular case of in-plane magnetization ($s_1^\perp = s_2^\perp = 1$ and $\varphi_1 = \varphi_2 = 0$), dealt with in Ref. 12, the energy $E^{(\text{DDI})}$ in Eq. (5) reduces to

$$E = -\lambda \mathbf{s}_1 \cdot \mathcal{D}_{12} \cdot \mathbf{s}_2. \quad (7)$$

In fact, we may obtain a ferromagnetic or an antiferromagnetic in-plane ordering with $\mathbf{s}_1 \cdot \mathcal{D}_{12} \cdot \mathbf{s}_2 = \mathbf{s}_1 \cdot \mathbf{s}_2 - 3(\mathbf{s}_1 \cdot \mathbf{e}_{12}) \cdot (\mathbf{s}_2 \cdot \mathbf{e}_{12}) = \pm 1$, or an out-of-plane ordering along the bond \mathbf{e}_{12} with the energy $\mathbf{s}_1 \cdot \mathcal{D}_{12} \cdot \mathbf{s}_2 = \mp 2$.

B. Disks

For the setup in Fig. 1 (b and c) with two disk-shaped magnets of radius R and (center-to-center) distance D apart, the DI energy was computed in Refs. [56,57] upon including the shape function to account for the fact that the dipole-dipole approximation is no longer valid for close enough magnets of arbitrary shape. Each of these two cases was considered with both in-plane and out-of-plane magnetization. In order to write the corresponding expression of the DI energy in a compact form we introduce the notation $\boldsymbol{\rho} = (r \cos \varphi_\rho, r \sin \varphi_\rho, z)$, $\rho^2 = r^2 + z^2$. We also introduce the vector \mathbf{p} for bookkeeping the shape parameters of the disks, *i.e.* $\mathbf{p} = (R, \tau)$ with $\tau = t/R$, $2t$ being the disk thickness. For arbitrary orientations of the two magnetic moments, the energy of the system is expressed in terms of the integrals $\mathcal{S}_n(r, z; \mathbf{p})$, $n = 1, 2, 3$ given in Eqs. (39, 40, 41) of Ref. 57. In general, they can only be computed numerically.

In the case of the vertical setup [Fig. 1b], *i.e.* ($z = D, r = 0, \varphi_\rho = 0$), with arbitrary orientations of the two magnetic moments, we find that the energy can be written as (the subscript ‘‘VD’’ stands for vertical disks)

$$E_{\text{VD}}^{(\text{Int})} = \lambda \left[\cos(\varphi_1 - \varphi_2) s_1^\perp s_2^\perp - 2s_1^z s_2^z \right] \quad (8)$$

where the coefficient λ is now given by

$$\lambda = \left(\frac{\mu_0}{4\pi}\right) \frac{M^2}{D^3} \times \mathcal{I}_d^v(\zeta, \tau). \quad (9)$$

Here the shape integral (for vertical disks) $\mathcal{I}_d^v(\zeta, \tau)$ reduces to⁵⁷

$$\mathcal{I}_d^v(\zeta, \tau) = 8\zeta^3 \tau \int_0^\infty \frac{dq}{q^2} J_1^2(q) e^{-2q\zeta\tau} [\cosh(2q\tau) - 1] \quad (10)$$

where we have introduced the dimensionless parameters

$$\zeta \equiv \frac{D}{2t}, \quad \tau = \frac{t}{R}$$

and $J_1(x)$ is the Bessel function of the first kind.

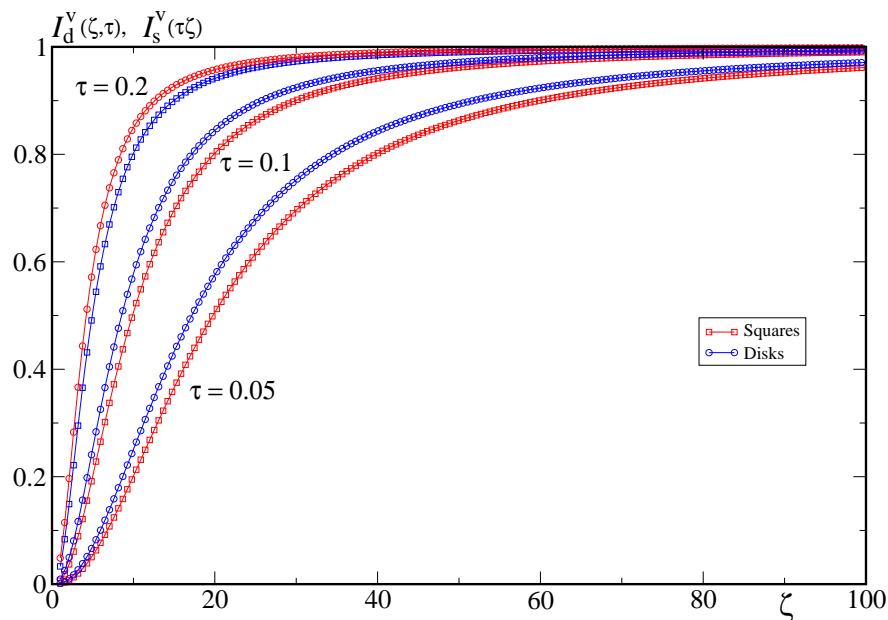


Figure 2: Shape integrals $\mathcal{I}_s^v(\tau\zeta)$ and $\mathcal{I}_d^v(\zeta, \tau)$ for the vertical setup of rectangular slabs or disks, as functions of the (dimensionless) distance ζ .

The two DI coefficients (6) and (9) for slabs and disks, respectively, can be compared upon noting that $\zeta = \delta/\tau$. So for a given τ we compare the corresponding shape integrals $\mathcal{I}_s^v(\tau\zeta)$ and $\mathcal{I}_d^v(\zeta, \tau)$, as functions of ζ . This is shown in Fig. 2. Note that $\mathcal{I}_d^v(\zeta, \tau)$ is a special case of the general integrals $\mathcal{S}_n(r, z; \mathbf{p})$, $n = 1, 2, 3$ introduced in Ref. 57. For elements of finite size, all integrals $\mathcal{S}_n(r, z; \mathbf{p})$, $n = 1, 2, 3$ approach 1 when the interaction approaches the pure dipolar interaction or the magnetic elements are replaced by point dipoles. In this case, $\lambda \rightarrow \left(\frac{\mu_0}{4\pi}\right) M^2/D^3$ which is indeed the coefficient of the dipole-dipole interaction [see Eq. (4)]. In Fig. 2 it is seen that $\mathcal{I}_s^v(\tau\zeta)$ and $\mathcal{I}_d^v(\zeta, \tau)$ do go to 1 as ζ goes to infinity, *i.e.* for a large distance between the two disks. On the other hand, for small ζ , or very large radius R , the integrals $\mathcal{I}_s^v(\tau\zeta)$ and $\mathcal{I}_d^v(\zeta, \tau)$ tend to zero as expected since then the DI vanishes between infinite thin layers. Finally, we see that as the aspect ratio τ increases, the two integrals increase and this implies that, for a fixed distance D , the interaction is stronger between thicker magnets.

For the horizontal setup in the xy plane with an arbitrary angle φ_ρ between the dimer's bond and the x axis, *i.e.* ($z = 0, r = D, \varphi_\rho$), we have the energy for the dipolar interaction

$$E_{\text{HD}}^{(\text{Int})}/\lambda = [\cos(\varphi_1 - \varphi_2) - (2 + \Phi) \cos(\varphi_1 - \varphi_\rho) \cos(\varphi_2 - \varphi_\rho)] s_1^\perp s_2^\perp + \Phi s_1^z s_2^z. \quad (11)$$

with

$$\lambda = \left(\frac{\mu_0}{4\pi}\right) \frac{M^2}{D^3} \times \mathcal{I}_d^h(\zeta, \tau) \quad (12)$$

and $\Phi(\zeta, \tau) \equiv \mathcal{J}_d^h(\zeta, \tau) / \mathcal{I}_d^h(\zeta, \tau)$. $\mathcal{I}_d^h(\zeta, \tau)$ and $\mathcal{J}_d^h(\zeta, \tau)$ are two shape integrals given by⁵⁷

$$\begin{aligned} \mathcal{I}_d^h(\zeta, \tau) &= 16\zeta^2\tau \int_0^\infty \frac{dq}{q^2} J_1^2(q) J_1(2\zeta\tau q) \left[1 - \frac{(1 - e^{-2q\tau})}{2q\tau} \right], \\ \mathcal{J}_d^h(\zeta, \tau) &= 16\zeta^3\tau \int_0^\infty \frac{dq}{q^2} J_1^2(q) J_0(2\zeta\tau q) (1 - e^{-2\tau q}). \end{aligned} \quad (13)$$

Note that the energy (11), especially with $\varphi_\rho = \pi/2$, is of the same form as (5) and (8) but with different coefficients for the transverse and longitudinal components of the magnetic moments. This reflects the fact that in the horizontal setup, the dimer's bond is not along the axis of the rotational symmetry of the disks. The horizontal setup in Fig. 1c corresponds to the configuration ($z = 0, r = D, \varphi_\rho = \pi/2$) with the dimer's bond along the y axis. In section III B, we investigate the FMR characteristics for the horizontal dimer with a bond along the x axis, *i.e.* with $\varphi_\rho = 0$ and $e_{12} \parallel e_x$. This choice is motivated by the relative ease in analyzing the various stationary points of the total energy and the consequent simplicity of the derivation of the corresponding analytical expressions for the eigenfrequencies.

C. Total energy

Collecting all contributions (and dividing by KV) we obtain the total (dimensionless) energy of the magnetic dimer

$$\mathcal{E} = \mathcal{E}^{(\text{free})} + \mathcal{E}^{(\text{Int})}$$

where $\mathcal{E}^{(\text{free})}$ is given in Eq. (2).

For two magnets uniformly magnetized in arbitrary directions, $\mathcal{E}^{(\text{Int})}$ is given by Eq. (5) for the vertical stack of rectangular slabs (upon dividing by KV), by Eq. (8) for the two disks along the z axis and by Eq. (11) for the two disks on the same xy plane. In fact, the three cases can be encompassed in the following compact form, which is a generalization of the dipole-dipole interaction (4)

$$\mathcal{E}^{(\text{Int})} = \xi [\mathbf{s}_1 \cdot J \mathbf{s}_2 - 3\psi (\mathbf{s}_1 \cdot \mathbf{e}_{12}) (\mathbf{s}_2 \cdot \mathbf{e}_{12})]. \quad (14)$$

The diagonal ‘‘exchange matrix’’ J and the coefficient ψ are given by

$$\begin{cases} J = I, & \psi = 1, & \text{vertical setup,} \\ J = \begin{pmatrix} 1 & 0 & 0 \\ 0 & 1 & 0 \\ 0 & 0 & \Phi \end{pmatrix}, & \psi = \frac{2+\Phi}{3} & \text{horizontal setup.} \end{cases} \quad (15)$$

For convenience, we have also defined the (dimensionless) coupling constant $\xi \equiv \lambda / (KV)$ which explicitly reads

$$\xi = \left(\frac{\mu_0}{4\pi}\right) \frac{M^2/D^3}{KV} \times \begin{cases} \mathcal{I}_s^v(\delta), & \text{vertical slabs,} \\ \mathcal{I}_d^v(\zeta, \tau), & \text{vertical disks,} \\ \mathcal{I}_d^h(\zeta, \tau), & \text{horizontal disks.} \end{cases}$$

Therefore, the magnetic state of the dipolar-coupled dimer is obtained by minimizing, with respect to the angles θ_i, φ_i , the total energy given by the combined equations (2, 14).

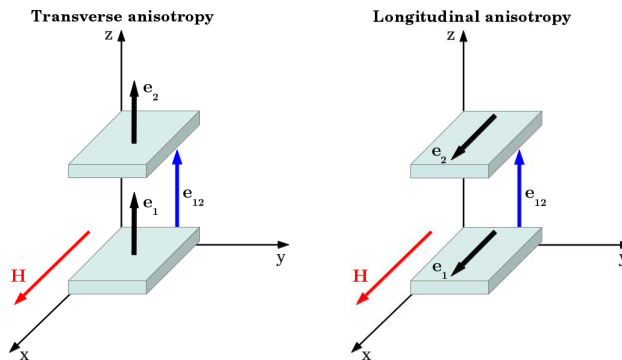


Figure 3: Magnetic dimer setup with transverse anisotropy on the left and longitudinal anisotropy on the right. The nonmagnetic spacer is not shown.

III. FMR CHARACTERISTICS

We consider three situations regarding the orientation of the (effective) anisotropy easy axes within the magnetic elements, with respect to both the applied field and the dimer's bond e_{12} . The magnetic field will be varied both in magnitude and direction. Then, the two anisotropy easy axes e_1, e_2 will be either (for the vertical dimer)

- parallel to each other but perpendicular to the applied field, which is parallel to the dimer's bond, and this setup will be referred to as the transverse anisotropy (TA). This is the easy-axis geometry [see Fig. 3 (left)].
- parallel to each other and to the applied field and thus perpendicular to the dimer's bond e_{12} , a situation that will be referred to as the longitudinal anisotropy (LA). The easy axes lie in the plane of the magnetic elements. This is the easy-plane geometry [see Fig. 3 (right)].

Longitudinal and transverse here refer to the orientation with respect to the applied field [see Fig. 3]. We will also consider the case of mixed anisotropy (MA), *i.e.* with the easy axis of one of the magnetic layers along the field and the other perpendicular to it.

For the horizontal setup we also consider the cases of longitudinal and transverse anisotropy, together with a situation usually studied experimentally where the direction of the applied field and that of the anisotropy easy axes are interchanged.

In order to compute the FMR characteristics (resonance frequency and resonance field), for a given configuration of the system under study, we use the standard method for a system of many degrees of freedom, namely we first determine the absolute minimum of the total energy for the given setup of the system. Then, we linearize the Landau-Lifshitz equation near this minimum leading to an eigenvalue problem. We solve the latter for a fixed (in direction and amplitude) magnetic field to obtain the eigenfrequencies, *i.e.* the resonance frequencies which are functions of the applied field and all other physical parameters. In addition, the results obtained in this work have been recovered using the general theory of magnetic oscillations in antiferromagnets and ferrimagnets [see *e.g.* chapter 3 of the textbook 60] which also proceeds by linearizing the equations of motion upon writing the magnetic moments and the effective fields as sums of steady and alternating components, assuming the latter to be small as compared to the former. Then setting to zero the determinant of the ensuing (eigenvalue) scalar equations, one establishes the characteristic equation for the frequencies of free oscillations. For zero damping the solutions of this equation yield the eigenfrequencies. On the other hand, the eigenvectors of this eigenvalue problem correspond to the eigenmodes of the system. Thus, for the particular case of a magnetic dimer, one obtains the so-called *binding* and *anti-binding modes*.

For a fixed frequency the eigenvalue problem can be solved for the magnetic field and this yields the resonance field as a function of the direction of the applied field in addition to the other materials parameters. Depending on the situation, the eigenvalue problem may be solved analytically thus rendering analytical expressions for the resonance frequencies. This is the case for LA and TA. However, for MA and, in general, the problem can only be solved numerically. In this case, some care is necessary when determining the absolute minimum of the whole system. In our work, we combine a Metropolis algorithm to (roughly) find the magnetic moment direction that corresponds to the global minimum and then use the Landau-Lifshitz equation with small damping to zero in on the absolute minimum, *i.e.* we do a down-hill search of the minimum⁶¹.

For the task at hand in this work, namely the calculation of FMR spectra of magnetic dimers with different configurations, we now give a few orders of magnitude of the various parameters involved. These are the magnetic field, the (effective) uniaxial anisotropy, and the inter-layer DI coupling.

- slab (or rectangular) films: these may represent two thin Co or Fe layers separated by a nonmagnetic spacer a few nanometers thick. The (intra-layer) anisotropy constant (per unit area) is $K_s \sim 3.56 \times 10^{-5} \text{ J/m}^2$ and the isotropic exchange coupling is $J \sim 2 \times 10^{-2} \text{ J/m}^2$. Then, the DI coupling evaluates to $\lambda \sim 3 \times 10^{-4} \text{ J/m}^2$.
- Disks (or thin cylinders): we consider the system studied in Refs. 55,63. The authors study a system of three pairs of twin disks of FeV of diameter $2R$ with a center-to-center distance D placed on the same plane [Fig 1 c]. The disks are perpendicularly magnetized (along the z axis) by an external field $\mu_0 H = 1.72 \text{ T}$ and the saturation magnetization is $M_0 \simeq 1.45 \times 10^6 \text{ A/m}$. The disks order in a bcc crystal structure⁶³ and their anisotropy constant and exchange coupling were estimated to be $K \simeq 4.1 \times 10^4 \text{ J/m}^3$, $J = Aa_0 \simeq 8.6 \times 10^{-20} \text{ joules}$. The disks are of radius $R = 300 \text{ nm}$ and thickness $2t = 26.7 \text{ nm}$, and are separated by a center-to-center distance $D = 800, 1000, 1200 \text{ nm}$. Then, for the shortest distance $D = 800 \text{ nm}$ the coefficient in Eq. (11) evaluates to $\lambda = \left(\frac{\mu_0}{4\pi}\right) M^2/D^3 \simeq 2.36 \times 10^{-17} \text{ joules}$ and thereby $\xi \simeq 0.076$. For $D = 1000 \text{ nm}, 1200 \text{ nm}$ we respectively have: $\xi \simeq 0.039, 0.023$.

A word is in order regarding the normalization of the frequency. Starting from the Landau-Lifshitz equation we may divide by the anisotropy field H_a and then define the dimensionless time $t_1 \equiv t/t_s$ where t_s is the characteristic time of the underlying material given by $t_s = (\gamma H_a)^{-1}$, with $\gamma \simeq 1.76 \times 10^{11} (\text{Ts})^{-1}$ being the gyromagnetic factor. For the FeV disks, for instance, $t_s \simeq 10^{-10} \text{ s}$. Therefore, we later use the notation $\tilde{\omega} \equiv \omega \times t_s = \omega / (\gamma H_a)$ for the dimensionless frequency and for a frequency ν (in GHz) we write $\nu \simeq 10 \text{ GHz} \times \tilde{\omega} / (2\pi)$.

A. Vertical dimer

We compute the resonance frequency as a function of the magnitude of the magnetic field and the resonance field and the dimer's coupling as a function of the applied field polar angle θ_h with $0 \leq \theta_h \leq \pi$ for a fixed azimuthal angle $\varphi_h = 0$. So the field is rotated in the xz plane.

1. Transverse anisotropy (TA)

The magnetic field is along the x axis ($\theta_h = \pi/2$) and the anisotropy axes are parallel to the MD bond \mathbf{e}_{12} [see Fig. 3 left]. By minimizing the total energy comprising the two contributions in Eq. (2) and Eq. (14) with respect to the two polar angles $\theta_i, i = 1, 2$, we obtain the energy global minimum

$$\begin{cases} \sin \theta_1 = \sin \theta_2 = \frac{2h}{2k+3\xi/2}, & h \leq h_c, \\ \theta_1 = \theta_2 = \frac{\pi}{2}, & h > h_c \end{cases} \quad (16)$$

where the critical magnetic field h_c is given by

$$h_c = k + \frac{3}{2}\xi \quad (17)$$

or in S.I. units $H_c = H_a + 3\lambda/M$.

For $h = h_c$ there is a change of regime, namely from a regime where the magnetic field is dominating thus forcing the two magnetic moments to lie along its direction (x), and the regime where there is a competition between, on one hand, the magnetic field along the x axis and, on the other, the effective field along the z axis comprising the anisotropy and DI contributions.

The resonance frequencies for TA are

$$\tilde{\omega}_{\text{res}}^+ \equiv \left(\frac{\omega}{\gamma H_a}\right)_{\text{res}}^+ = \begin{cases} \sqrt{(2k+3\xi)^2 - (2h)^2}, & h \leq h_c, \\ \sqrt{(2h)^2 - 2h(2k+3\xi)}, & h > h_c. \end{cases} \quad (18)$$

for the first mode and

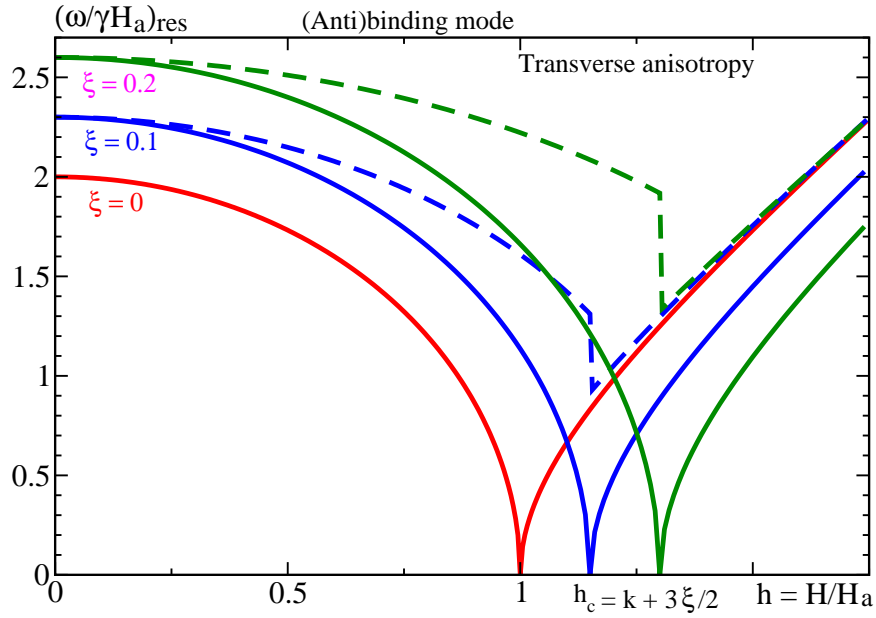


Figure 4: Resonance frequency of the binding mode (continuous lines) and the anti-binding mode (dashed lines) as a function of the magnetic field and varying dipolar interlayer coupling, with transverse anisotropy.

$$\tilde{\omega}_{\text{res}}^- \equiv \left(\frac{\omega}{\gamma H_a} \right)_{\text{res}}^- = \begin{cases} \sqrt{\frac{(2h)^2}{3} \left[1 - 4 \left(\frac{2k}{2k+3\xi} \right)^2 \right] + (2k+3\xi)^2}, & h \leq h_c, \\ \sqrt{(2h-2\xi)(2h-2k+\xi)}, & h > h_c. \end{cases} \quad (19)$$

for the second mode.

Let us now briefly analyze the corresponding eigen-oscillations. When the two magnetic moments are brought together, the mutual interaction of their (degenerate) resonances or modes can induce a splitting of the modes into pairs characterized by the so-called binding/anti-binding states. To see this, one writes the magnetic moment M_i as a sum of the equilibrium component $M_i^{(0)}$ and an alternating component m_i (assumed to be small compared to the former), *i.e.* $M_i \simeq M_i^{(0)} + m_i$, $i = 1, 2$. Then, upon solving the linearized (coupled) equations of motion for the two vectors m_i , $i = 1, 2$ one obtains the eigen-frequencies and the corresponding eigen-vectors (modes) of the system. In the present situation, for the mode with frequency $\tilde{\omega}_{\text{res}}^+$ we obtain $m_1^y = m_2^y$ and $m_1^z = m_2^z$, *i.e.* the two vectors m_1 and m_2 are identical and as such they precess together. This is the uniform mode or the *binding mode*. On the other hand, at the frequency $\tilde{\omega}_{\text{res}}^-$ one gets $m_1^y = -m_2^y$ and $m_1^z = -m_2^z$, which implies that $m_2 = -m_1$, and this corresponds to the *anti-binding mode*. It is clear that in the absence of coupling ($\xi = 0$) the two frequencies become degenerate (equal). For instance, setting $\xi = 0$ in the first line of Eqs. (18, 19) renders the (doubly degenerate) resonance frequency of a single magnetic moment

$$\tilde{\omega}_{\text{res}}^\pm (\xi = 0) = 2\sqrt{k^2 - h^2}. \quad (20)$$

Similarly, in zero field ($h = 0$) the effective field is along the MD bond. Indeed, the DI energy is minimized when the two magnetic moments are parallel to each other and pointing along the vector e_{12} , which is also the direction of the MD effective anisotropy axis. In this case, the resonance frequency reads [from Eqs. (18, 19)]

$$\tilde{\omega}_{\text{res}}^\pm (h = 0) = 2k + 3\xi.$$

Let us now discuss the behavior of the resonance frequency as we vary the applied field h and DI intensity ξ . We do so only for the rectangular slabs since the change in the case of disks is only of a little quantitative impact.

In Fig. 4 we plot the frequency $\tilde{\omega}_{\text{res}}^+$ in continuous curves and $\tilde{\omega}_{\text{res}}^-$ in dashed curves, against the field magnitude, for different values of the DI interlayer coupling. $\tilde{\omega}_{\text{res}}^- (\xi = 0)$ is not plotted as it coincides with $\tilde{\omega}_{\text{res}}^+ (\xi = 0)$.

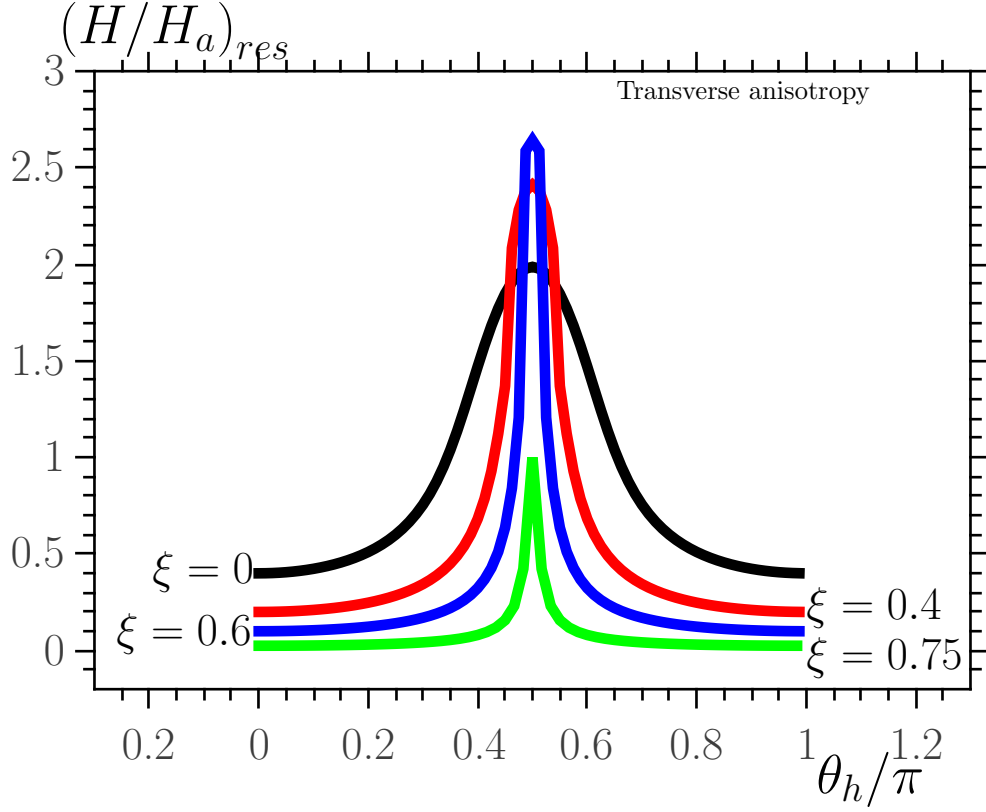


Figure 5: Resonance field as a function of the magnetic field direction for the frequency $\tilde{\omega} = 2.8$ (~ 28 GHz) and varying dipolar interlayer coupling, for the magnetic trilayer with transverse anisotropy.

We first discuss the behavior of the frequency $\tilde{\omega}_{\text{res}}^+$. The results are similar to the case of uniaxial anisotropy^{60,61} in a transverse field but the curves are now shifted by the DI contribution that brings an additional anisotropy. As explained above, this is due to the fact that for the present MD setup, the DI and uniaxial anisotropy have additive effects leading to a (larger) effective anisotropy field perpendicular to the magnetic field. Similarly to the case of uniaxial anisotropy the resonance frequency goes to zero at some critical value h_c of the applied field. This is usually used to determine the anisotropy field from experiments. In the present case, this could be used to determine the strength of the interlayer coupling between two magnetic layers of known anisotropy. For a magnetic field above the saturation value, Eq. (18) yields $\tilde{\omega}_{\text{res}}^+ \rightarrow 2h$, which corresponds to the straight line seen at high fields in Fig. 4. In this binding mode, the two magnetic moments remain parallel to each other and the magnetic dimer behaves like a single magnetic moment but with larger stiffness due to the DI coupling. This is why the curve $\tilde{\omega}_{\text{res}}(h)$ is similar to that of a single magnetic moment but with an increasing h_c as a function of the dimer's coupling.

Turning now to the frequency $\tilde{\omega}_{\text{res}}^-$ we have two main observations, in comparison with the frequency $\tilde{\omega}_{\text{res}}^+$. First, the anti-binding mode frequency is higher than that of the binding mode, as is usually the case. Indeed, the anti-binding mode is an excitation of the system that is higher in energy than the binding mode, considered as the ground state. In this mode we have $\mathbf{m}_2 = -\mathbf{m}_1$ and thereby the two magnetic moments M_i , $i = 1, 2$ do not remain parallel to each other, thus leading to a “negative” contribution to the effective anisotropy. This in turn induces a decrease of the critical point h_c with increasing coupling, as can be seen by extrapolating to lower fields the dashed straight lines in Fig. 4. Moreover, from Eq. (19) we can see that under high fields the resonance frequency $\tilde{\omega}_{\text{res}}^-$ becomes independent of the coupling.

The issue of binding and anti-binding modes and their comparison is rather involved and requires a thorough analysis. For example, a more precise investigation of these modes and their dynamics can be achieved by computing (both analytically and numerically) the time evolution of the two magnetic moments on- and off-resonance upon varying the applied field and the coupling. In order not to make the present article too bulky, with the risk of drowning its main message, in the sequel we restrict our discussion to the binding modes and their characteristics, leaving the analysis of anti-binding modes for a separate work.

In Fig. 5 we show the results for the resonance field for the same setup as in Fig. 4, for a fixed frequency $\tilde{\omega}$. The valley and the peak correspond to the easy and hard directions, respectively. We see that as the DI increases the effect of the easy direction is enhanced leading to a wider valley and a lower resonance field. The effect of the hard direction is also enhanced but affects a narrower range of field directions around $\theta = \pi/2$. In summary, as the DI increases the easy axis range widens whereas that of the hard axis shrinks. The fact that the amplitude of the resonance field globally decreases when the DI increases is simply due to the fact that with a stronger effective field, a smaller magnetic field is needed to satisfy the resonance condition.

2. Longitudinal anisotropy (LA)

The magnetic field is still along the x axis ($\theta_h = \pi/2$) but now the anisotropy axes are parallel to it but perpendicular to the MD bond e_{12} [see Fig. 3 right]. In this case, the DI and uniaxial anisotropy contributions induce different preferred directions for the two magnetic moments and thereby they are in competition with each other. Therefore, the two magnetic moments may be parallel or anti-parallel to each other and lie in the xz plane. Denoting by θ the polar angle they make to the z axis, the MD energy then reads $\mathcal{E} = -4h \sin \theta - \sin^2 \theta + \xi (1 - 3 \cos^2 \theta)$ and upon minimizing it with respect to θ we obtain the following minima: $\theta = \pm\pi/2$ or $\sin \theta = 2h/(3\xi - 2k)$. Hence, we have the following three distinct states with their respective energies

$$\theta_1 = \frac{\pi}{2} = \theta_2, \quad \mathcal{E}_1 = -2h - 2k + \xi, \quad (21a)$$

$$\theta_1 = \frac{\pi}{2} = -\theta_2, \quad \mathcal{E}_2 = -2k - \xi, \quad (21b)$$

$$\sin \theta_1 = \frac{2h}{3\xi - 2k} = \sin \theta_2, \quad \mathcal{E}_3 = -\frac{(2h)^2}{3\xi - 2k} - 2\xi. \quad (21c)$$

Note that for the last state to exist ξ must satisfy $\xi \geq \frac{2}{3}(k+h) \equiv \xi_{\min}$. The antiferromagnetic state (21b), with $M_1 = -M_2$, results from the fact that the DI tends to align the magnetic moments in an anti-parallel configuration when they are normal to the DI bond. Hence, the transition from the ferromagnetic state (21a) along the field direction to the antiferromagnetic state (21b), still along the field direction, occurs when ξ reaches the value h . Next, as the DI increases the system undergoes the transition from the antiferromagnetic state (21b) to the (oblique) ferromagnetic state (21c), tilted towards the MD bond, when ξ crosses the value

$$\xi_{\text{tilt}} \equiv \frac{2}{3} \left[(2k) + \sqrt{k^2 - 3h^2} \right], \quad (22)$$

obtained by setting $\mathcal{E}_2 = \mathcal{E}_3$.

The system then selects one minimum or the other according to the strength of the magnetic field as compared to the other two energy contributions. More precisely, we have two field regimes separated by the saturation field $h_s = k/2$, which is obtained by solving $\mathcal{E}_1 = \mathcal{E}_2$ for $\xi = \xi_{\min}$.

Therefore, we have the following cases:

1. For a weak field, $h \leq h_s$, a comparison of DI to both the field and the anisotropy contributions, yields three regimes:

- (a) for weak coupling $\xi < h$, the field is strong enough to drive the two magnetic moments along its direction (x axis). Hence the ferromagnetic state in Eq. (21a) is selected. The resonance frequency in this case is given by

$$\tilde{\omega}_{\text{res}} = \sqrt{(2k + 2h)(2k + 2h - 3\xi)}. \quad (23)$$

- (b) for intermediate coupling $h < \xi \leq \xi_{\text{tilt}}$, the anisotropy is still dominant but the DI contribution is stronger than the magnetic field contribution, thus leading to the antiferromagnetic state (21b) along the anisotropy axis. In this case, The resonance frequency reads

$$\tilde{\omega}_{\text{res}} = \sqrt{A - \sqrt{B}} \quad (24)$$

with $A \equiv (2h)^2 + (2k + \xi)^2 + 2\xi^2$ and $B \equiv 9\xi^2(2k + \xi)^2 + (2h)^2(4k + \xi)(4k + 3\xi)$.

(c) for a strong coupling, *i.e.* $\xi > \xi_{\text{tilt}}$, the system orders in the oblique ferromagnetic state (21c) and the resonance frequency is then given by

$$\tilde{\omega}_{\text{res}} = \frac{\sqrt{\xi}}{3\xi - 2k} \times \sqrt{(2h)^2(2k + 3\xi) - (2k - \xi)(3\xi - 2k)^2}. \quad (25)$$

- For strong fields $h > h_s$ there are only two regimes for the DI coupling. Indeed, since the latter competes with the magnetic field and thereby only the transition from state (21a) to the state (21c) takes place and this occurs when the DI coupling reaches the value $\xi = \xi_{\text{min}}$. Hence, for $\xi \leq \xi_{\text{min}}$ the system minimum is given by (21a) and the resonance frequency is the same as in Eq. (23). For $\xi > \xi_{\text{min}}$ the system orders in the global state (21c) and the corresponding resonance frequency is that given in Eq. (25).

Note that in standard FMR measurements one has to apply a sufficiently strong field, *i.e.* $h > h_s$, in order to saturate the magnetic system which then occupies an energy minimum. This would mean in the present work that the regime with $h \leq h_s$ found above, and included here for completeness, might not be relevant to all systems studied by the FMR technique. For instance, in Ref. 55, the applied field is $H = 1.72$ T while $H_a \simeq 0.056$ T.

In Fig. 6 we plot the FMR frequency against the DI coupling ξ . The upper panel is for the case $h = 0$, included as a reference. In this particular case, there is a competition between the DI and the (effective) uniaxial anisotropy so that when ξ increases there occurs a transition from the state (21b) to the state (21c) at $\xi = 2k$. Therefore, for $\xi \leq 2k$ the minimum is at $\theta_1 = \frac{\pi}{2} = -\theta_2$ and the resonance frequency reads $\tilde{\omega}_{\text{res}} = \sqrt{2k - \xi}$ whereas for $\xi > 2k$ the minimum is at $\theta_1 = \theta_2 = 0, \pi$ and the resonance frequency becomes $\tilde{\omega}_{\text{res}} = \sqrt{\xi(\xi - 2k)}$. In the case $h < h_s$, the middle panel exhibits the three regimes found above. In the first regime the two magnetic moments are in a ferromagnetic state and the FMR frequency decreases as ξ increases. In the second regime, the two magnetic moments are antiferromagnetic and precess in opposite directions. The FMR frequency again decreases when ξ increases. Finally, in the third regime the two magnetic moments are again parallel to each other and the FMR frequency increases with ξ towards the asymptote $\xi = h$, similarly to the case of a single magnetic moment. On the other hand, for $h > h_s$ (lower panel) the FMR plots exhibit two distinct regimes with a particular value of ξ for which ω_{res} goes to zero.

In Fig. (7) we plot the resonance field for $\tilde{\omega} = 2.8$ against the field polar angle θ_h . This presents the evolution of the competition between the DI and uniaxial anisotropy as the former is increased. For low values of ξ the uniaxial anisotropy dominates and thereby imposes the direction of the system's effective easy axis ($\theta_h = \pi/2$). As the interaction further increases the DI axis becomes easier while the anisotropy axis becomes harder. This induces a "cone-like" behavior of the easy axis for high values of DI [see the curve with $\xi = 1$, where the easy axis now comprises a wider range of θ_h as compared to the curve with $\xi = 0$]. The difference in the behavior of the hard axis for $\xi = 0.5$ is due to the different nature of the DI contribution to the effective anisotropy, when compared to that of the uniaxial anisotropy. The DI turns out to have a stronger effect along the direction perpendicular to the MD bond, inducing a hard axis at a much faster rate than the one it induces for the easy axis in the parallel direction.

3. Mixed anisotropy

Here we deal with the situation where one of the magnetic layers has an easy axis anisotropy and the magnetization then points normal to the layer's plane, whereas the second magnetic layer has an easy-plane magnetization. More precisely, we set $e_1 \parallel e_z$ and $e_2 \parallel e_x$. Whereas for the longitudinal and transverse configurations analytical expressions have been obtained for the resonance frequency, in the present situation the analytical expressions for the stationary points are too cumbersome for practical use. For this reason, they have been computed numerically. Note that the different orientations of the easy axes may be a consequence of different thicknesses. This means that the two magnetic layers are not identical, as it has been assumed hitherto. A difference in the amplitude of the two magnetic moments will have a quantitative impact on the results, *e.g.* shifts in critical values. However, in the sequel we ignore this difference and concentrate on the qualitative behavior of the dimer.

The DI magnetic dimer with mixed anisotropy is somewhat similar to that with longitudinal anisotropy, insofar as the DI again competes with a longitudinal uniaxial anisotropy, but now it does so against only the contribution (to anisotropy) of one of the layers, thus decreasing (for $h = 0$) the critical value of ξ from $2k$ to $2k/\sqrt{3}$.

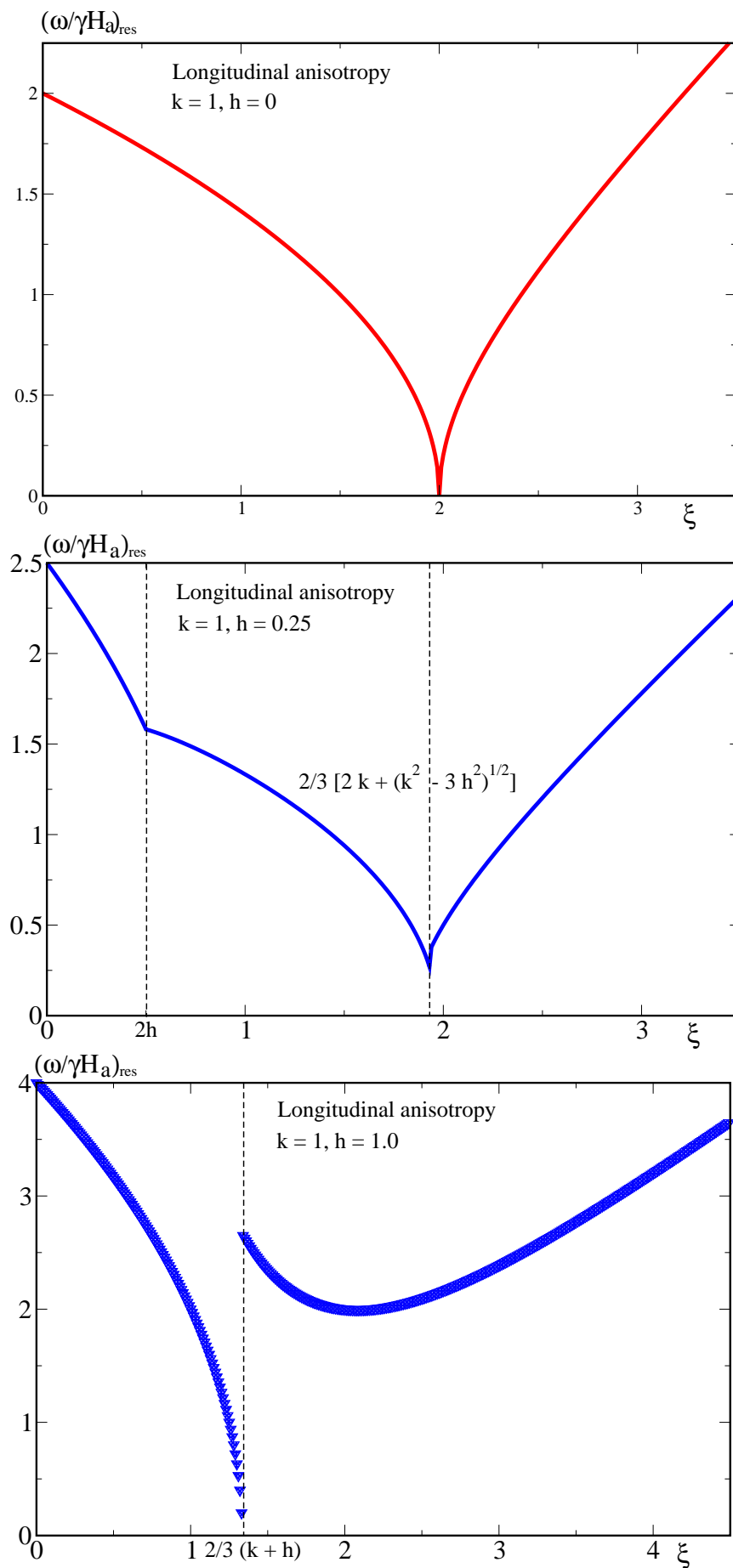


Figure 6: Resonance frequency against the interlayer DI coupling ξ for the values of the applied field h marking the three regimes discussed in the text.

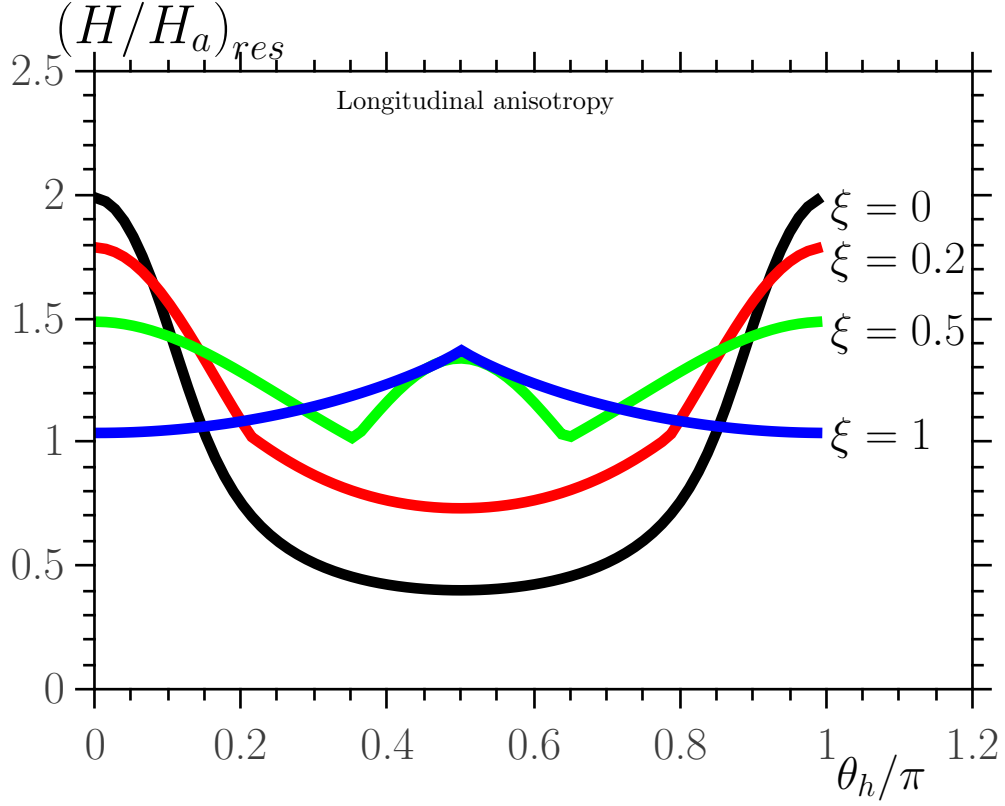


Figure 7: Resonance field as a function of the magnetic field direction in the xz plane for the frequency $\tilde{\omega} = 2.8$ and varying DI interlayer coupling and longitudinal anisotropy.

In Fig. 8, we see that in the absence of the interlayer coupling ($\xi = 0$), the effective easy axis is located somewhere between the two (layers) anisotropy axes (the individual anisotropy axes are seen as hard axes because of the competition between them). As the DI becomes stronger the precession around the direction $\theta_h = \pi/2$ becomes unfavorable and the precession angle decreases, while the precession around the MD bond becomes easier with a wider range of values for the field direction. The easy axis effectively starts to shift towards the MD bond until the interaction is strong enough to completely overcome the effect of the transverse component of the anisotropy. For $\xi = 0.75$ the interaction-anisotropy competition leads to a wide easy cone around the z axis, where H_{res} is almost constant. We again observe the enhanced hard axis behavior induced by the DI along the transverse direction. By further increasing the interaction ($\xi = 1$) we again observe the peak at $\theta_h = \pi/2$ and a clear easy axis along the MD bond. This implies that the longitudinal component of the anisotropy is no longer the most relevant contribution to the system and the dynamics is governed only by DI, and to a lesser extent, by the transverse anisotropy.

Fig. 9 shows a comparison of the FMR frequency as a function of the dipolar interaction parameter ξ for the three anisotropy configurations, in the absence of magnetic field ($h = 0$). We see that for $\xi = 0$ the frequencies start from the same value which indicates that the contribution of the uniaxial anisotropy is the same for the three configurations of the anisotropy axes. This changes as ξ increases since the effect of DI depends on the anisotropy configuration. For a magnetic dimer with TA, $\tilde{\omega}_{\text{res}}$ is a monotonically increasing function of ξ while the LA and MA configurations clearly exhibit the competition between the uniaxial anisotropy and DI. The critical value of ξ (denoted here by ξ_c^{FMR}) at which $\tilde{\omega}_{\text{res}} = 0$, and that depends on the configuration of the system, represents the value of the DI at which the competing anisotropy and interaction fields compensate for each other. The competing fields for each anisotropy configuration are: i) for a DI magnetic dimer with LA, the two (uniaxial) anisotropy fields against the interaction field, and ii) for a DI magnetic dimer with MA, the longitudinal anisotropy field on one hand against the transverse anisotropy and interaction field, on the other. This explains why the critical value of ξ assumes a higher value for LA than for MA, as the interaction has to overcome a stronger competing field due to the anisotropy of both magnetic layers. When ξ exceeds the critical value ξ_c^{FMR} the system enters the strong coupling regime, where the FMR resonance of the three anisotropy

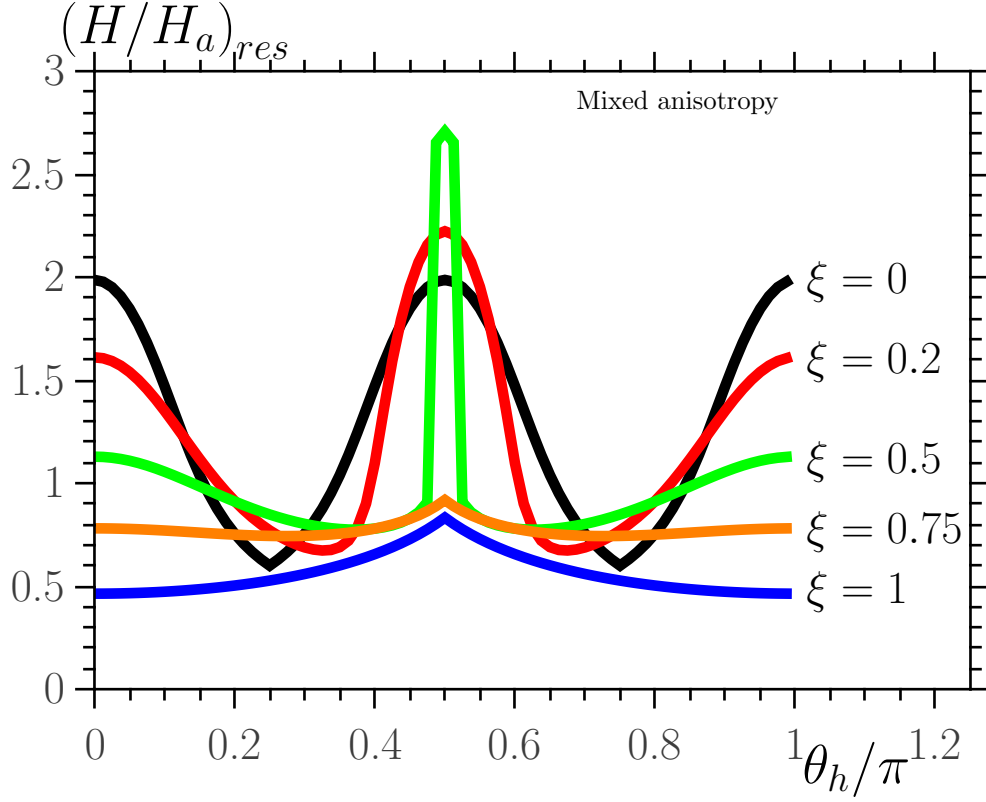


Figure 8: Resonance field vs field direction in the xz plane, with $\tilde{\omega} = 2.8$ and different values of the dipolar interaction in the MA configuration.

configurations behaves in a similar way again, differing only by an additive factor that depends on the nature of the competition between the anisotropy and the DI.

f(GHz)	TA	MA	LA
$\xi = 1$	13.5	3.97	6.36
$\xi = 3$	22.5	13.7	7.79

Table I: Resonance frequency for $\xi = 1$ and 3 for the three anisotropy configurations.

Table I gives the resonance frequency of cobalt layers for the three anisotropy configurations and two values of DI. $\xi = 1 < \xi_c^{\text{FMR}}$ and $\xi = 3 > \xi_c^{\text{FMR}}$ hold for TA, LA and MA. We clearly see that TA always leads to the fastest precession. LA precesses slightly faster than MA when $\xi < \xi_c^{\text{FMR}}$, and the MA precession is faster than that of the LA otherwise.

B. Horizontal dimer

Now, we deal with the horizontal setup of the magnetic dimer which, for convenience, we take here along the x axis, *i.e.* $e_{12} \parallel e_x$. This means that in Eq. (11) we set $\varphi_\rho = 0$. As discussed earlier, this choice makes it relatively easier to analyze the stationary points of the energy and to derive analytical expressions for the eigenfrequencies. Note that the energy expression (11) applies only to the case of a horizontal setup in the xy plane.

We only consider the case of two coupled disks. We treat two anisotropy configurations, either with the easy axes along the field direction x or perpendicular to the field, along the z direction. We also deal with the case of a field applied along the z axis and the two anisotropy axes along the x axis, as in the experimental study of

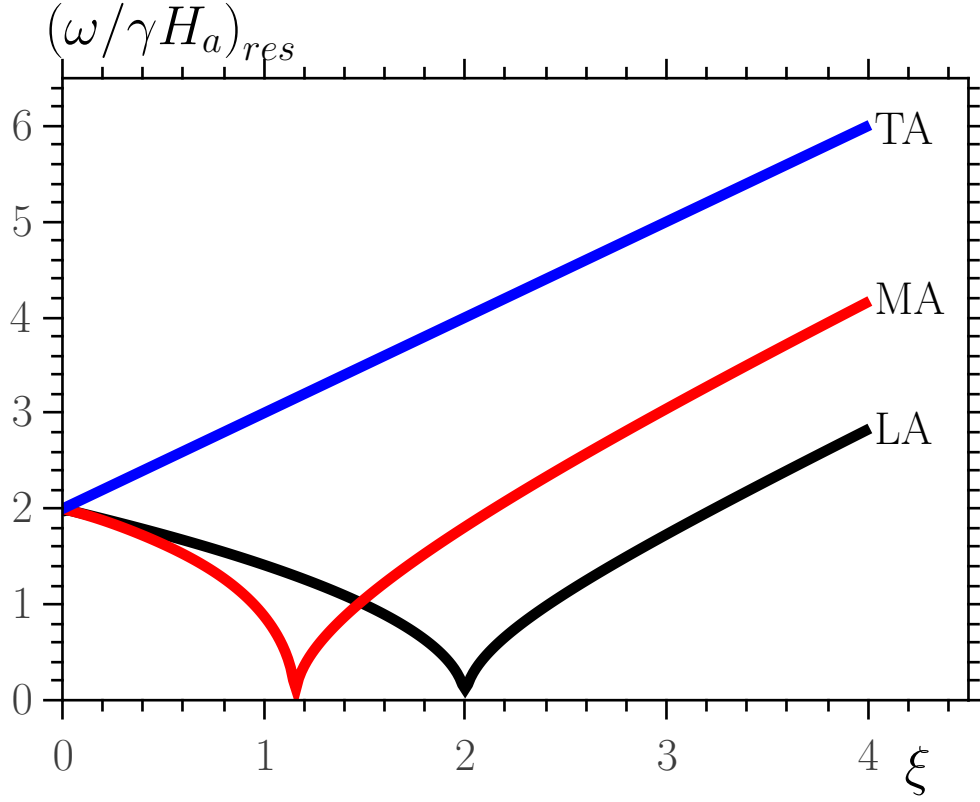


Figure 9: Resonance frequency for transverse, mixed, and longitudinal anisotropy configurations of the DI magnetic dimer.

Ref. 55 performed on FeV disks with aspect ratio $\tau = t/R \simeq 0.0445$ and $\zeta = D/2t \simeq 30$. For such parameters, $\Phi \simeq 0.58$.

1. *Easy axes parallel to the field (LA)*

The minimum in this case is simply given by

$$\theta_1 = \frac{\pi}{2} = \theta_2$$

because all the contributions to the effective field are along the x axis. The resonance frequency is then given by

$$\tilde{\omega}_{\text{res}} = \sqrt{(2h + 2k + \xi)(2h + 2k + \Phi\xi)} \quad (26)$$

An obvious consequence is the additive nature of the contributions from the applied field, the DI, and the anisotropy of this particular setup. Fig. 10 shows this additive effect through the fact that the resonance frequency is a monotonously increasing function of the applied field. Moreover, the effect of various values of the DI and the shape factor is merely to shift upwards the resonance frequency. This is incidentally in agreement with the results discussed earlier for the vertical dimer in that the DI induces a faster precession as it increases.

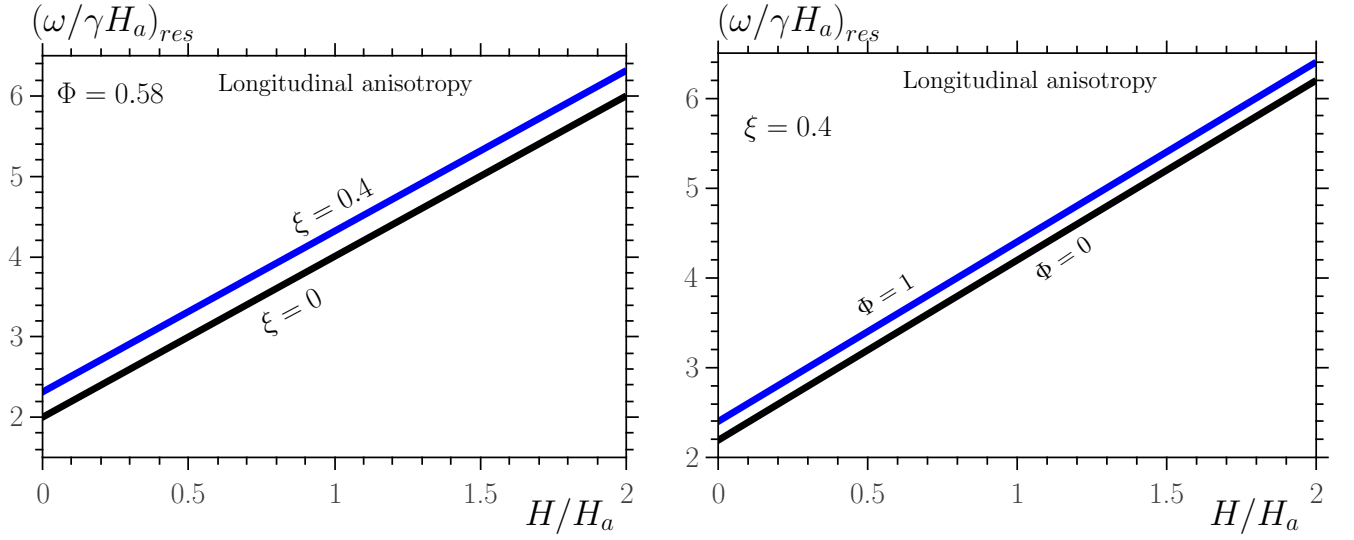


Figure 10: Resonance frequency for different values of the dipolar interaction ξ (left) and the shape factor Φ (right). The anisotropy easy axes are parallel to the applied field.

2. Easy axes perpendicular to the field (TA)

In this case, the minima of the system are

$$\begin{cases} \sin \theta_1 = \sin \theta_2 = \frac{2h}{2k-\xi}; & \cos \theta_1 = -\cos \theta_2, & h \leq h_c, \\ \theta_1 = \theta_2 = \frac{\pi}{2}, & & h > h_c. \end{cases} \quad (27)$$

Similarly to the vertical dimer, here again there is a minimal value $\xi_{\min} = 2k - 2h$ of the DI coupling ξ in order for the first state to exist. We may also consider this condition as leading to a critical value of the magnetic field given by $h_c = k - \xi/2$.

The corresponding resonance frequencies are (for the binding mode)

$$\tilde{\omega}_{\text{res}} = \begin{cases} \frac{1}{\sqrt{2k-\xi}} \sqrt{[(2k-\xi)^2 - (2h)^2]} [2k - (1-\Phi)\xi], & h \leq h_c, \\ \sqrt{(2h+\xi-2k)(2h+\Phi\xi)}, & h > h_c. \end{cases} \quad (28)$$

One should notice the additional dependence of the resonance frequency on the shape function Φ . However, the latter does not enter the energy minima of the system in Eq. (27).

Fig. 11 shows the resonance frequency as a function of the applied field for different values of ξ and Φ . It can be seen that increasing the DI decreases the critical value of the field at which the minimum of the system changes, since $h_c = k - \xi/2$. This is due to the fact that the minimum $\sin \theta_i = 2h/(2k - \xi)$ results from the competition between the anisotropy and the combined effect of the applied field and the DI. Thus, if the DI is stronger, a weaker field will be necessary to overcome completely the effect of the anisotropy. This is to be compared with Fig. 4 where the critical value $h_c = k + 3\xi/2$ increases with ξ . Therefore, if the anisotropy field of a material measured by FMR comes out smaller than that of the individual layers, the results above hints to the possibility of a non negligible DI acting at the interface.

3. Horizontal dimer with vertical magnetic field

A situation that is also of interest and which can be easily set up experimentally is the one where the orientations of the magnetic field and easy axes are swapped with respect to the previous case, *i.e.* $e_h \parallel e_z$ and

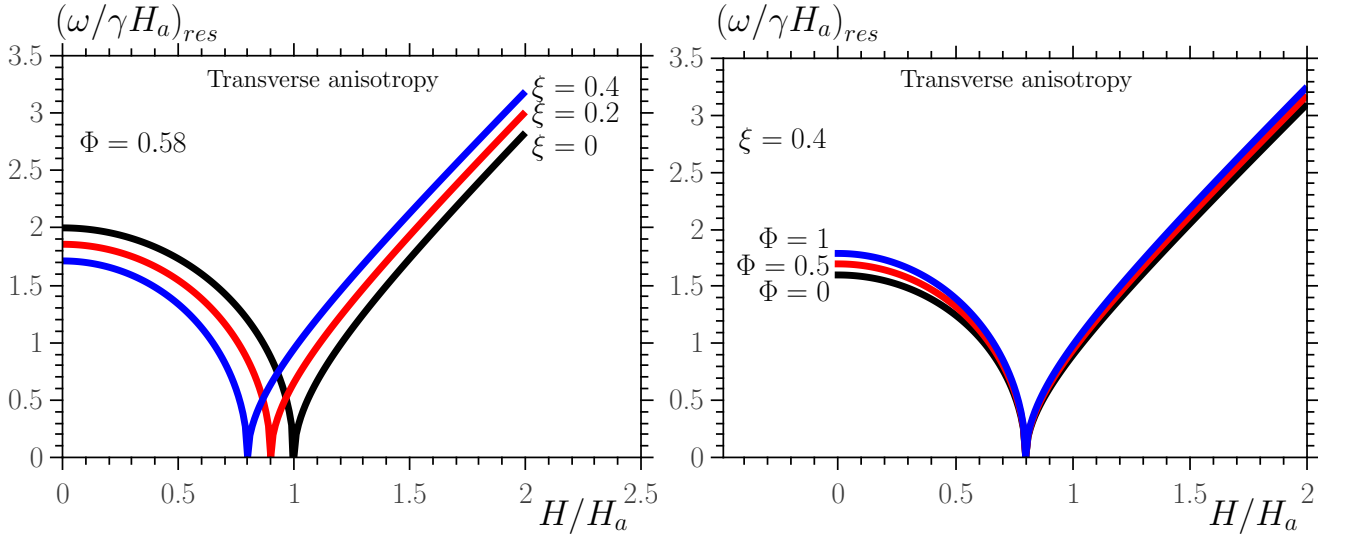


Figure 11: Resonance frequency for different values of the dipolar interaction ξ and the shape factor Φ . The anisotropy easy axes are perpendicular to the applied field.

$e_i \parallel e_x, i = 1, 2$. This was considered, for example, in the case of two coupled vertical disks of FeV^{54,55}. In this situation the energy minima of the magnetic dimer are given by

$$\begin{cases} \cos \theta_1 = \cos \theta_2 = \frac{2h}{2k + \xi(1 + 2\Phi)}, & h \leq h_c^{\text{TA}}, \\ \theta_1 = \theta_2 = 0, & h > h_c^{\text{TA}} \end{cases} \quad (29)$$

where now the critical value of the magnetic field is $h_c^{\text{TA}} = k + \xi(1 + 2\Phi)/2$.

Upon comparing the energy minima in Eqs. (27) and (29) we realize that a swap of the field direction and that of the anisotropy easy axes leads to a qualitatively different result. The reason is that, owing to the additional anisotropy induced by the dipolar interaction, having the dimer's bond parallel to the anisotropy easy axes leads to a stronger effective anisotropy than when the dimer's bond is perpendicular to them. Obviously, the corresponding resonance frequencies are also rather different.

For $h < h_c^{\text{TA}}$, the corresponding eigenvalues that yield the resonance frequencies read

$$\tilde{\omega}_{\text{res}}^1 = \frac{1}{2k + \xi(1 + 2\Phi)} \sqrt{[2k + \xi(1 + 2\Phi)]^2 (2k + \xi) - (2h)^2 [2k - \xi(1 + 2\Phi)]} (2k + \xi\Phi) \quad (30)$$

and

$$\tilde{\omega}_{\text{res}}^2 = \frac{1}{\sqrt{2k + \xi(1 + 2\Phi)}} \sqrt{[2k + \xi(1 + 2\Phi)]^2 - (2h)^2} [2k + \xi(2 + \Phi)]. \quad (31)$$

For $\xi = 0$ we have $\tilde{\omega}_{\text{res}}^1 = \tilde{\omega}_{\text{res}}^2$. However, for $\xi \neq 0$ the eigenvalue (30) is the resonance frequency of the fundamental mode and the eigenvalue (31) is the resonance frequency of the higher-order precession mode. Note that in general, the DI increases the resonance frequency of the higher-order mode while reducing that of the fundamental mode. However, in a horizontal magnetic dimer with TA this is not the case, and there is a mode crossing (or the modes are swapped) at a field $(h_c^{\text{TA}})^{\text{swap}}$ given by

$$(h_c^{\text{TA}})^{\text{swap}} = h_c^{\text{TA}} \times \sqrt{\frac{2k + \xi(1 + \Phi)}{4k + \xi(1 + 2\Phi)}} \quad (32)$$

obtained by setting $\tilde{\omega}_{\text{res}}^1 = \tilde{\omega}_{\text{res}}^2$. Note that $(h_c^{\text{TA}})^{\text{swap}} < h_c^{\text{TA}}$ since $\Phi > 1/2$ and usually $\xi < 2k$. This indicates that the eigenfrequency $\tilde{\omega}_{\text{res}}^1$ that corresponds to the fundamental mode for an applied field $h < (h_c^{\text{TA}})^{\text{swap}}$ becomes that of the higher-order mode for higher values of the field, where the frequency of the fundamental mode is then given by $\tilde{\omega}_{\text{res}}^2$. We may summarize the different regimes as follows

$$\tilde{\omega}_{\text{res}} = \begin{cases} \tilde{\omega}_{\text{res}}^1, & h < (h_c^{\text{TA}})^{\text{swap}}, \\ \tilde{\omega}_{\text{res}}^2, & (h_c^{\text{TA}})^{\text{swap}} < h < h_c^{\text{TA}}, \\ \sqrt{[2h - 2k - \xi(1 + 2\Phi)][2h + \xi(1 - \Phi)]}. & h > h_c^{\text{TA}}. \end{cases} \quad (33)$$

Note that for $k \neq 0$ and $h < h_c^{\text{TA}}$ the frequency of the non-interacting dimer ($\xi = 0$) given by Eq. (20) is easily recovered from the expressions above.

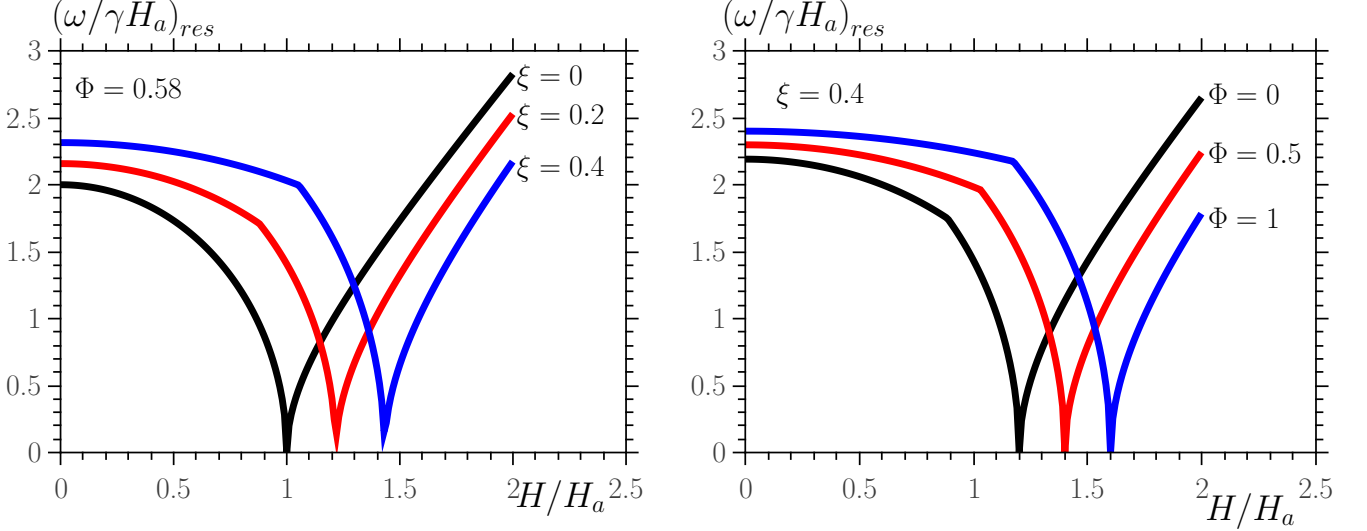


Figure 12: Resonance frequency for different values of the dipolar interaction ξ and the shape factor Φ .

Fig. 12 shows the resonance frequency as a function of the applied field for different values of ξ and Φ . The abrupt change in the slope of the curve observed for low values of the field marks the mode swap. It can be seen that with increasing DI, the resonance frequency increases for low values and decreases for high values of the applied field. At the same time, it increases the field critical value since $h_c^{\text{TA}} = k + \xi(1 + 2\Phi)/2$. The latter reduces to the critical value (17) for the vertical dimer with the same anisotropy configuration. Indeed, as we saw earlier for the vertical setup instead of the two integrals in Eq. (13) we only have the integral (10), which means that $\Phi \rightarrow 1$. The main difference between the two case, *i.e.* the vertical dimer with TA and the present case of the horizontal dimer is that in the former one has an out-of-plane anisotropy while in the latter the anisotropy is in plane and this explains the appearance of the shape factor Φ in the latter situation.

Furthermore, the plots in Fig. 12 (right) show that as Φ increases the frequency increases for low values and decreases for high values of the applied field, while increasing the field critical value. The effect of the shape on the resonance frequency is much more noticeable in this configuration than in the other ones dealt with earlier.

Fig. 13 shows the resonance field for the present configuration where it is clearly seen that the stronger is the DI contribution the flatter is the minimum corresponding to the direction along the dimer's bond and the lower is the resonance field. The reason, as was explained earlier, is the fact that the stronger is the dipolar interaction the smaller is the field necessary for the resonance condition.

In Ref. 55, for instance, the applied field is $H = 1.72$ T and this implies that the resonance frequency should be given by the last line in Eq. (33) and thereby the increment of the resonance frequency due to DI reads

$$\Delta\tilde{\omega}_{\text{DI}} = \sqrt{[2h - 2k - \xi(1 + 2\Phi)][2h + \xi(1 - \Phi)]} - \sqrt{2h(2h - 2k)}.$$

Then, for the experimentally observed⁵⁵ shift in frequency (induced by the dipolar interactions) of $\Delta\nu \simeq 50$ MHz, $\Delta\tilde{\omega}_{\text{DI}}/2\pi = \Delta\nu/10 \simeq 5 \times 10^{-3}$ or $\Delta\tilde{\omega}_{\text{DI}} \simeq 10\pi \times 10^{-3}$. The geometrical factors of the system studied yield $\Phi \simeq 0.58$ leading to the reduced parameter $\xi \simeq 0.082$ or the DI parameter $\lambda = \xi \times KV \simeq 5.56 \times 10^{-16}$ J, for the inter-elements distance $D = 800$ nm. This value of ξ is larger by the factor $\mathcal{I}_d^h(30, 0.0445) \simeq 1.1378$ than the

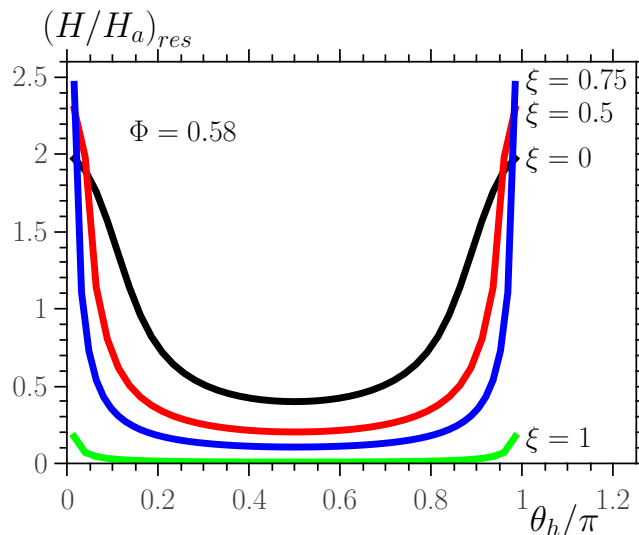


Figure 13: Resonance field for different values of the dipolar interaction ξ .

value that one would obtain within the dipole-dipole approximation where the nanomagnets are considered as point dipoles (for which $\mathcal{I}_d^h(\zeta, \tau) \rightarrow 1$). This means that in such a magnetic dimer, the inter-elements distance, or more precisely the parameter ζ is large enough for the dipole-dipole approximation to apply. However, for arbitrary shapes one has to take account of the aspect ratio and the more general formulas given here for the energy, its minima and the corresponding resonance frequencies.

IV. CONCLUSION

In this work we have developed a unified formalism for analyzing the ferromagnetic spectrum of a magnetic dimer, representing either a trilayer with a nonmagnetic spacer or a pair of nanomagnets (platelets or nanoparticles) coupled by dipolar interaction. This formalism goes beyond the dipole-dipole approximation of point dipoles since it fully takes account of the finite size and aspect ratio of the magnetic nano-elements.

We have provided analytical expressions for the ferromagnetic resonance frequency in various regimes of the applied field and inter-element dipolar coupling, in various configurations of the anisotropy of the two magnetic elements. Among the results that can be easily inferred from these analytical developments is that when the field is applied normal to the dimer's bond and to the anisotropy easy axes, in either a vertical or a horizontal setup, the critical value of the magnetic field at which the resonance frequency vanishes is an increasing function of the coupling parameter; and it depends on the shape factor in the case of in-plane anisotropy in the horizontal setup. In the horizontal setup with transverse anisotropy, this critical value decreases for more strongly coupled dimers. On the other hand, in the case of longitudinal anisotropy there is no critical value at all and the resonance frequency is a monotonously increasing function of the applied field. These features provide an unambiguous means for characterizing the anisotropy and the inter-element coupling in magnetic dimers.

We have also studied numerically the effects of these physical parameters on the resonance field in the various regimes. In the vertical setup, a variation of the dimer's dipolar coupling, which can be achieved by changing the material and thickness of the spacer, can lead to a change of the direction of the effective anisotropy. This is seen through a drastic change in the curves of the resonance field versus the direction of the applied magnetic field as the inter-layer coupling is increased. These curves are of course routinely obtained in standard FMR measurements and could help characterize the effective anisotropy and coupling in such magnetic dimers.

Comparison of the expressions and the other results obtained here with experiments using the standard FMR with fixed frequency, or a network-analyzer with varying frequency and magnetic field, yields a valuable means to characterize the dipolar coupling in systems of two magnetic moments. In addition, an interacting dimer is the building block for a multi-element system such as magnetic multilayers or assemblies of magnetic nanoparticles. For example, in order to investigate the FMR characteristics of an assembly of magnetic nanoparticles (spatially organized or not) deposited on a nonmagnetic substrate or embedded in a nonmagnetic insulating matrix, one could reinstate in all the analytical expressions given here the particle's index i and its volume

V_i together with the inter-particle (center-to-center) distance r_{ij} . Then, upon summing over the distributions of the volume and the lattice distances r_{ij} , one could derive new expressions for the resonance frequencies for the assembly. The latter could then be evaluated upon computing the ensuing lattice sums or expanded into approximate practical expressions in the case of dilute assemblies.

-
- ¹ P. Grünberg, R. Schreiber, Y. Pang, M. B. Brodsky, and H. Sowers, Phys. Rev. Lett. **57**, 2442 (1986).
 - ² E. F. Kneller and R. H. Hawig, IEEE Trans. Magn. **27**, 3588 (1991).
 - ³ A. Fert, P. Grünberg, A. Barthélémy, F. Petroff, and W. Zinns, J. Magn. Magn. Mater. **1**, 140 (1995).
 - ⁴ R. H. Victora, X. Shen, IEEE Trans. Magn. **41**, 537 (2005).
 - ⁵ D. Suess, T. Schrefl, R. Dittrich, M. Kirschner, F. Dorfbauer, G. Hrkac, J. Fidler, J. Magn. Magn. Mater. **290**, 551 (2005).
 - ⁶ G. Woltersdorf, O. Mosendz, B. Heinrich, and C. H. Back, Phys. Rev. Lett. **99**, 246603 (2007).
 - ⁷ B. Hillebrands and K. E. Ounadjela, *Spin Dynamics in Confined Magnetic Structures I* (Springer, 2002).
 - ⁸ P. Bruno, Ph.D. thesis, Université de Paris Sud (1989).
 - ⁹ E. W. Hill, S. L. Tomlinson, and J.-P. Li, J. Appl. Phys. **73**, 5978 (1993).
 - ¹⁰ P. Bruno, Phys. Rev. B **52**, 411 (1995).
 - ¹¹ K. Xia, W. Zhang, M. Lu, and H. Zhai, Phys. Rev. B **55**, 12561 (1997).
 - ¹² P. Vargas and D. Altbir, Phys. Rev. B **62**, 6337 (2000).
 - ¹³ B. Heinrich, Y. Tserkovnyak, G. Woltersdorf, A. Brataas, R. Urban, and G. E. W. Bauer, Phys. Rev. Lett. **90**, 187601 (2003).
 - ¹⁴ P. Wang, W. K. Shen, J. M. Bai, R. H. Victora, J. H. Judy, and W. L. Song, Appl. Phys. Lett. **86**, 142504 (2005).
 - ¹⁵ D. Suess, T. Schrefl, S. Faehler, M. Kirschner, G. Hrkac, F. Dorfbauer, and J. Fidler, Appl. Phys. Lett. **87**, 012504 (2005).
 - ¹⁶ D. Suess, T. Schrefl, M. Kirschner, G. Hrkac, F. Dorfbauer, O. Ertl, and J. Fidler, Appl. Phys. Lett. **41**, 3166 (2005).
 - ¹⁷ G. N. Kakazei, Yu. G. Pogorelov, M. D. Costa, V. O. Golub, J. B. Sousa, P. P. Freitas, S. Gardoso, and P. E. Wigen, J. Appl. Phys. **97**, 10A723 (2005).
 - ¹⁸ B. Skubic, E. Holmström, D. Iuşan, O. Bengone, O. Eriksson, R. Brucas, B. Hjörvarsson, V. Stanciu, and P. Nordblad, Phys. Rev. Lett. **96**, 057205 (2006).
 - ¹⁹ K. C. Schuermann, J. D. Dutson, S. Z. Wu, S. D. Harkness, B. Valcu, H. J. Richter, R. W. Chantrell, and K. O'Grady, J. Appl. Phys. **99**, 08Q904 (2006).
 - ²⁰ G. Woltersdorf and Ch. H. Back, Phys. Rev. Lett. **99**, 227207 (2007).
 - ²¹ A. Berger, N. Supper, Y. Ikeda, B. Lengsfeld, A. Moser, and E. E. Fullerton, Appl. Phys. Lett. **93**, 122502 (2008).
 - ²² M. Madami, S. Tacchi, G. Gubbiotti, G. Carlotti, H. Pandana, R. D. Gomez, H. Tanigawa, and T. Ono, J. Appl. Phys. **104**, 063510 (2008).
 - ²³ L. Sun, P. Wong, W. Zhang, X. Zou, L. Luo, Y. Zhai, J. Wu, Y. Xu, and H. Zhai, J. Appl. Phys. **109**, 033913 (2011).
 - ²⁴ A. F. Franco, and H. Kachkachi, J. Phys.: Condens. Mat. **25**, 316003 (2013).
 - ²⁵ M.P. Sharrock, IEEE Trans. Magn. **26**, 193 (1990).
 - ²⁶ K.E. Johnson, J. Appl. Phys. **69**, 4932 (1991).
 - ²⁷ J.-L. Dormann, D. Fiorani, and E. Tronc, Adv. Chem. Phys. **98**, 283 (1997).
 - ²⁸ X. Batlle and A. Labarta, J. Phys. D: Appl. Phys. **35**, R15 (2002).
 - ²⁹ P. Tartaj, P. Morales, S. Veintemillas-Verdaguer, T. Gonzalez-Carreño, and C. Serna, J. Phys. D: Appl. Phys. **36**, R182 (2003).
 - ³⁰ J.L. Dormann, L. Bessais, and D. Fiorani, J. Phys. C **21**, 2015 (1988).
 - ³¹ S. Morup and E. Tronc, Phys. Rev. Lett. **72**, 3278 (1994).
 - ³² H. Mamiya and I. Nakatani, J. Magn. Magn. Mater. **177**, 966 (1998).
 - ³³ J.-L. Dormann, and D. Fiorani, J. Magn. Magn. Mater. **202**, 251 (1999).
 - ³⁴ D. V. Berkov and N. L. Gorn, J. Phys.: Condens. Matter **13**, 9369 (2001).
 - ³⁵ P.E. Jonsson and J.L. Garcia-Palacios, Phys. Rev. B **64**, 174416 (2001).
 - ³⁶ P. Allia, M. Coisson, P. Tiberto, F. Vinai, M. Knobel, M. A. Novak, and W. C. Nunes, Phys. Rev. B **64**, 144420 (2001).
 - ³⁷ H. Mamiya, I. Nakatani, and T. Furubayashi, Phys. Rev. Lett. **88**, 067202 (2002).
 - ³⁸ O. Iglesias and A. Labarta, Phys. Rev. B **70**, 144401 (2004).
 - ³⁹ O. Chubykalo-Fesenko and R.W. Chantrell, J. Appl. Phys. **97**, 10J315 (2005).
 - ⁴⁰ S. H. Masunaga, R. F. Jardim, P. F. P. Fichtner, and J. Rivas, Phys. Rev. B **80**, 184428 (2009).
 - ⁴¹ D. Ledue and R. Patte and H. Kachkachi, J. Nanoscience and Nanotechnology **12**, 4953 (2012).
 - ⁴² Z. Sabsabi, F. Vernay, O. Iglesias, H. Kachkachi, Phys. Rev. B **169**, 323 (2013).
 - ⁴³ K.B. Urquhart, B. Heinrich, J.F. Cochran, A.S. Arrott, and Myrtle, J. Appl. Phys. **64**, 5334 (1988).
 - ⁴⁴ B. Heinrich and J.F.C. Cochran, Adv. Phys. **42**, 523 (1993).
 - ⁴⁵ B. Heinrich, in *Ultrathin magnetic structures II*, edited by B. Heinrich and J. Bland (Springer-Verlag, Berlin, 1994), p. 195.
 - ⁴⁶ M. Farle, Rep. Prog. Phys. **61**, 755 (1998).
 - ⁴⁷ J.F. Cochran, in *Ultrathin magnetic structures II*, edited by B. Heinrich and J. Bland (Springer-Verlag, Berlin, 1994), p. 222.

- ⁴⁸ C. Mathieu, J. Jorzick, A. Frank, S. O. Demokritov, A. N. Slavin, B. Hillebrands, B. Bartenlian, C. Chappert, D. Decanini, F. Rousseaux, et al., *Phys. Rev. Lett.* **81**, 3968 (1998).
- ⁴⁹ E. Beaupaire, J.-C. Merle, A. Daunois, and J.-Y. Bigot, *Phys. Rev. Lett.* **76**, 4250 (1996).
- ⁵⁰ B. Koopmans, M. van Kampen, J. T. Kohlhepp, and W. J. M. de Jonge, *Phys. Rev. Lett.* **85**, 844 (2000).
- ⁵¹ M. van Kampen, C. Jozsa, J. T. Kohlhepp, P. LeClair, W. J. M. de Jonge, and B. Koopmans, *Phys. Rev. Lett.* **88**, 227201 (2002).
- ⁵² J. Stöer and H. C. Siegmann, *Magnetism: from fundamentals to nanoscale dynamics* (Springer, Berlin, 2006).
- ⁵³ Y. Zhu, *Modern techniques for characterizing magnetic materials* (Kluwer Academic Publishers, Boston, 2005).
- ⁵⁴ V.V. Naletov, G. de Loubens, G. Albuquerque, S. Borlenghi, V. Cros, G. Faini, J. Grollier, H. Herdequint, *Phys. Rev. B* **84**, 224423 (2011).
- ⁵⁵ B. Pigeau, C. Hahn, G. de Loubens, V.V. Naletov, O. Klein, K. Mitsuzuka, D. Lacour, M. Hen, S. Andrieu, and F. Montaigne, *Phys. Rev. Lett.* **109**, 247602 (2012).
- ⁵⁶ S. Tandon, M. Beleggia, Y. Zhu, and M. De Graef, *J. Magn. Magn. Mater.* **271**, 9 (2004).
- ⁵⁷ M. Beleggia, S. Tandon, Y. Zhu, and M. De Graef, *J. Magn. Magn. Mater.* **278**, 270 (2004).
- ⁵⁸ P. Bruno, *J. Magn. Soc. Jpn* **15**, 15 (1991).
- ⁵⁹ P. Bruno and J.-P. Renard, *J. Magn. Magn. Mater.* **135**, 343 (1994).
- ⁶⁰ A.G. Gurevich and G.A. Melkov, *Magnetization oscillations and waves* (CSC Press, Florida, 1996).
- ⁶¹ H. Kachkachi and D. S. Schmool, *Eur. Phys. J. B* **56**, 27 (2007).
- ⁶² D. Altbir, M. Kiwi, R. Ramírez, and I. K. Schuller, *J. Magn. Magn. Mater.* **149**, L246 (1995).
- ⁶³ K. Mitsuzuka, D. Lacour, M. Hehn, S. Andrieu, and F. Montaigne, *Appl. Phys. Lett.* **100**, 192406 (2012).